Controlling the superconducting transition by spin-orbit coupling

N. Banerjee,[1,2] J.A. Ouassou,[3] Y. Zhu,[2] N.A. Stelmashenko,[2] J. Linder,[3] and M.G. Blamire[2]

[1]*Department of Physics, Loughborough University, Epinal Way, Loughborough, LE11 3TU, United Kingdom*
[2]*Department of Materials Science and Metallurgy, University of Cambridge, 27 Charles Babbage Road, Cambridge, CB3 0FS, United Kingdom*
[3]*Center for Quantum Spintronics, Department of Physics, Norwegian University of Science and Technology, NO-7491 Trondheim, Norway*

Whereas there exists considerable evidence for the conversion of singlet Cooper pairs into triplet Cooper pairs in the presence of inhomogeneous magnetic fields, recent theoretical proposals have suggested an alternative way to exert control over triplet generation: intrinsic spin-orbit coupling in a homogeneous ferromagnet coupled to a superconductor. Here, we proximity-couple Nb to an asymmetric Pt/Co/Pt trilayer, which acts as an effective spin-orbit coupled ferromagnet owing to structural inversion asymmetry. Unconventional modulation of the superconducting critical temperature as a function of in-plane and out-of-plane applied magnetic fields suggests the presence of triplets that can be controlled by the magnetic orientation of a single homogeneous ferromagnet. Our studies demonstrate for the first time an active role of spin-orbit coupling in controlling the triplets – an important step towards the realization of novel superconducting spintronic devices.

I. INTRODUCTION

Conventional superconductivity emerges from an attractive pairing of spin-up and spin-down electrons, whereas ferromagnetism arises due to an imbalance in the number of spin-up and spin-down electrons. In superconductor/ferromagnet (S/F) proximity structures, the competing nature of these two orders is the source of rich physics [1, 2]. For example, the two electrons in a conventional Cooper pair enter different spin bands upon transmission into an adjacent F layer, resulting in a finite centre-of-mass momentum. This causes a weak oscillatory dependence of the superconducting transition temperature T_c, which is superimposed on the monotonic T_c suppression due to increasing F layer thickness [3, 4]. In more complex F/S/F trilayers, T_c is higher when the F moments are antiparallel than parallel [1, 5–7], arising from the higher net pair-breaking exchange field in the parallel state. This spin-switch effect allows an active control of T_c using magnetic states.

In contrast, S/F/F and F/S/F systems have recently shown an enhancement in the proximity effect between the S and the F layers [8–11] for non-collinear F-moment alignments. This unusual proximity effect results from conventional spin-zero singlet Cooper pairs being transformed into spin-one triplet pairs. These long-ranged triplets (LRTs) consist of electrons from the same spin band, and are therefore immune to a pair-breaking exchange field in F oriented along the spin-polarization of the Cooper pairs, enhancing the coupling between the layers. The increased coupling makes superconductivity spread across the whole system, reducing T_c by up to 120–400 mK [8, 10, 12]. Although the control of superconductivity by modulating magnetic states is attractive for applications in superconducting spintronics [13–17], precisely controlling the angle between the magnetic layers is difficult [8–10, 17–19]. Practical applications require a simplified structure with fewer interfaces to minimize spin-scattering, motivating the exploration of alternative mechanisms for triplet generation. Theoretical studies [20–27] predict that spin-orbit coupling (SOC) in S/F bilayers can produce an anisotropic depairing effect on triplets. The Cooper pair spin direction being determined by the F layer moment, then implies that in an S/F bilayer with SOC, triplets can be controlled by the magnetisation direction of a single homogeneous magnet [25]. In this paper, we report measurements on Nb/Pt(x)/Co/Pt proximity structures, where the structural inversion asymmetry gives rise to a Rashba coupling for $x > 0$ [28, 29]. We compare the $T_c(H)$ behaviour between samples with and without SOC to demonstrate the role of a triplet proximity effect in the former, and confirm the prediction that T_c can be controlled by rotating a single homogeneous magnetic layer in SOC systems.

The structure of this paper will be as follows. We start by giving a brief theoretical discussion of the proposed mechanism in Section II, which serves to motivate the experiment. In Section III, we then describe the experimental setup and measurements, demonstrating a spin-valve effect with only one homogeneous ferromagnet. These results are then compared to numerical simulations based on the Usadel equation in Section IV, and further interpreted and discussed in Section V.

II. THEORY

In the quasiclassical and diffusive limits, superconductivity is well-described by the so-called Usadel diffusion equation [39]. Near the critical temperature T_c, the superconducting pair amplitudes go to zero, meaning that the diffusion equation can be linearized with respect to pair amplitudes near this transition. In materials with superconductivity, ferromagnetism, and spin-orbit coupling, the linearized diffusion equations are [25]:

$$iD\nabla^2 f_s = \epsilon f_s + \boldsymbol{h}\boldsymbol{f}_t - \Delta, \tag{1}$$

$$iD\nabla^2 \boldsymbol{f}_t = \epsilon \boldsymbol{f}_t + \boldsymbol{h} f_s + 2iD\boldsymbol{\Omega}\boldsymbol{f}_t, \tag{2}$$

where f_s is the singlet pair amplitude, $\boldsymbol{f}_t$ the triplet pair amplitude, D the diffusion coefficient, ϵ the quasiparticle energy, Δ the superconducting gap, $\boldsymbol{h}$ the exchange field, and $\boldsymbol{\Omega}$ is a 3×3 matrix that describes the effects of the spin-orbit coupling.

From these equations alone, we can understand a lot about the system behaviour. When the superconducting gap Δ is

nonzero, Eq. (1) implies that there has to be singlet pairs f_s in the system as well. Indeed, it is precisely these singlet pairs that form the superconducting condensate of a conventional superconductor like Nb in the first place. Next, in the presence of an exchange field $\boldsymbol{h}$, some of these singlets f_s are converted into triplets $\boldsymbol{f}_t$ according to Eq. (2). Note that the direction of the triplet vector $\boldsymbol{f}_t$ parametrizes the spins of the pair, and $\boldsymbol{f}_t$ is proportional to the conventional $\boldsymbol{d}$-vector [23]. The triplets generated here are oriented along the exchange field ($\boldsymbol{f}_t \parallel \boldsymbol{h}$), and are known as *short-ranged triplets* (SRT) in the literature since they are exposed to the pair-breaking effects of the exchange field. Finally, Eq. (2) show that the triplet pairs are then affected by the spin-orbit matrix $\boldsymbol{\Omega}$. Depending on the structure of this matrix, the triplet pairs can either be rotated into LRT or just be suppressed by the pair-breaking effect of the spin-orbit coupling.

For a Rashba coupling in the xy-plane, i.e. broken inversion symmetry along the z-axis, $\boldsymbol{\Omega}$ becomes diagonal [25],

$$\boldsymbol{\Omega} = \alpha^2 \begin{pmatrix} 1 & 0 & 0 \\ 0 & 1 & 0 \\ 0 & 0 & 2 \end{pmatrix}, \tag{3}$$

where α is the Rashba coefficient. The fact that this matrix is diagonal implies that the spin-orbit coupling does not facilitate any conversion between SRT and LRT. Note that this is different from the case of both Rashba and Dresselhaus coupling, and also different from the nonlinear equations (required when $T \ll T_c$). The spin-orbit coupling shifts the effective energies of the in-plane (IP) triplets f_x, f_y by $2iD\alpha^2$, and for the out-of-plane (OOP) triplets f_z by $4iD\alpha^2$. This energy penalty is twice as large for OOP compared to IP triplets, and since the triplets are again oriented along the exchange field $\boldsymbol{h}$, we note that the triplet energy penalty can effectively be adjusted by rotating the exchange field.

To make this manifest, let us parametrize the exchange field

$$\boldsymbol{h} = h\,(\cos\theta\,\boldsymbol{e}_x + \sin\theta\,\boldsymbol{e}_z), \tag{4}$$

with θ being a parameter that rotates the field from IP to OOP. We can then project Eqs. (1) and (2) along the exchange field, obtaining the scalar diffusion equations

$$iD\,\nabla^2 f_s = \epsilon f_s + h f_t - \Delta, \tag{5}$$

$$iD\,\nabla^2 f_t = E_t f_t + h f_s, \tag{6}$$

where we have defined the effective triplet energy

$$E_t(\theta) = \epsilon + iD\alpha^2(3 - \cos 2\theta)\,. \tag{7}$$

This effective energy rotates between $\epsilon + 2iD\alpha^2$ and $\epsilon + 4iD\alpha^2$ depending on the magnetization angle θ. But we again note that the origin of this magnetic field dependence is that the spin-orbit coupling suppresses triplets oriented OOP more than triplets oriented IP; the magnetic field dependence only appears because the magnetic field controls what triplets we generate.

This magnetically tunable energy penalty lies at the core of the T_c control discussed in this paper. By increasing the triplet energy E_t, we can directly suppress the triplet amplitude in the effective ferromagnet, thus closing the triplet proximity channel. Because this implies that fewer pairs will leak out of the superconductor, the singlet amplitude in the superconductor goes up, and this restores T_c to higher levels.

Note that the *spin-valve effect*, i.e. the variation of the critical temperature T_c with the magnetization direction θ, is not a monotonic function of the spin-orbit coupling α. If α is very low, then *neither* energy penalty $2iD\alpha^2$ or $4iD\alpha^2$ is high enough to significantly suppress triplets, and T_c is low for all magnetic configurations. However, if α is very high, then *both* energy penalties are high enough to strongly suppress triplets, and T_c is high for all magnetic configurations. It is for intermediate values of α that the spin-valve effect is maximized.

III. EXPERIMENT

The thin-film stacks were deposited by DC magnetron sputtering in an ultrahigh vacuum chamber onto unheated oxidized Si(100) substrates placed on a rotating table. The substrates passed under magnetrons whose power, and the rotation speed of the substrate table, were adjusted to control the layer thicknesses (thicknesses in nanometers in parentheses below). The Pt and Co layer thicknesses were adjusted to tune the IP and OOP magnetic anisotropy, allowing control over the angle between the magnetization and sample plane by applying moderate magnetic fields, and so control the effectiveness of the singlet/triplet conversion. During deposition, the chamber was cooled by a liquid nitrogen jacket to achieve a pressure below 3×10^{-7} Pa. The layers were sputtered in 1.5 Pa Ar. Control samples of Nb/Pt and Nb/Co/Pt, as well as samples with varying Pt and Nb thickness, were also deposited. Figure 1(a,b) shows magnetization M vs. applied field H for Nb(24)/Co(1.5)/Pt(1.5) and Nb(24)/Pt(2)/Co(1.5)/Pt(1.5), which was measured at 10 K using a SQUID magnetometer. The blue and red points, respectively, represent the magnetic field applied in the IP and OOP directions. While for the Nb/Co/Pt stack the magnetization preferentially lies IP [Fig. 1(a)], insertion of a 2 nm Pt layer at the Nb/Co interface [Fig. 1(b)] results in a clear hysteretic switching for IP and OOP applied fields. This allows us to control the magnetization tilt with respect to the film plane using moderate magnetic fields. Perpendicular magnetic anisotropy in Pt/Co systems [30, 31] is

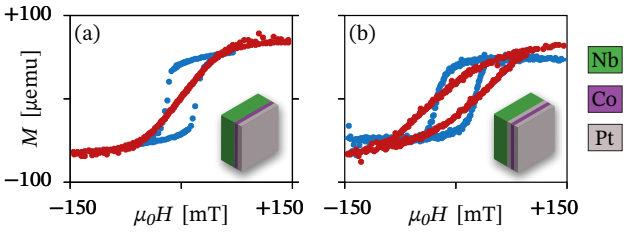

FIG. 1: Magnetisation M as a function of the applied field H for (a) Nb(24)/Co(1.5)/Pt(1.5) and (b) Nb(24)/Pt(2.0)/Co(1.5)/Pt(1.5). The blue and red points show the results for IP and OOP applied fields, respectively. The insets show the stack sequence.

generally attributed to an enhancement in the perpendicular Co orbital moment resulting from a Pt(5d)–Co(3d) hybridization. The OOP anisotropy is inversely proportional to the Co layer thickness [32], and a 1.5 nm Co layer allows us to control the tilt using low magnetic fields. Transport measurements were performed on unpatterned samples in the range of 3–8 K using four-point resistance measurement technique in a pulsed-tube cryocooler. The critical temperature T_c was defined as the temperature corresponding to 50% of the resistive transition. A constant bias current of 5 μA was used. The magnetic field was applied by starting at zero and ramping it up in 5–10 mT steps, and each T_c measurement was carried out in constant field. The maximum transition width was $\sim$180 mK.

Figure 2 shows $T_c(H)$ for the three different samples. For most of the samples there is an apparent difference between $T_c(0)$ for IP and OOP measurements likely arising due to the different relative positions of the sample holders with respect to the temperature sensor. Several measurements from the same sample shows that this difference in $T_c(0)$ is random and field-independent, and does not affect the overall trends of the $T_c(H)$ curve. This possibly arises due to minor differences in steady-state gas flow conditions between each cooling cycle.

Figure 2(a,b) shows $T_c(H)$ for a Nb(24)/Pt(2) bilayer and Nb(24)/Co(1.5)/Pt(1.5) trilayer in an IP field. Except for $\sim$15 mK background noise, we find that T_c remains roughly constant up to $H = 120$ mT. Figure 2(c) shows corresponding measurements for the Nb(24)/Pt(2)/Co(1.5)/Pt(1.5) stack. Strikingly, we find a rapid 40 mK suppression of the critical temperature between 0–100 mT. The full data range for all three samples shows that the T_c suppression below 100 mT for Nb(24)/Pt(2)/Co(1.5)/Pt(1.5) is comparable to the T_c suppression for the other two structures for the entire field range up to 500 mT (data not shown). While the net constant field-induced T_c suppression of $\sim$60 mK till 500 mT for all the structures can be explained by a weak field-induced depairing for 24 nm thick Nb films, the explanation for the T_c suppression by 40 mK at low fields for the structure with an additional Pt interlayer is not straightforward. From the systematic layer sequences, it is clear that the extra Pt layer between Nb and Co plays a role. For the OOP fields [Fig. 2(d–f)], all samples show a pronounced T_c suppression due to the strong orbital depairing from the applied field.

Before attempting to explain our results in terms of SOC-induced control of triplets, we rule out two other possibilities. Firstly, domain-wall induced suppression of superconductivity can be ruled out since at higher fields elimination of domain walls should restore superconductivity. This is in sharp contrast to Fig. 2(c), where superconductivity is suppressed at larger IP fields. Secondly, we quantify the flux-induced T_c modulation which arises from the OOP magnetization of Co-containing samples [Fig. 2(e,f)]; for the Nb/Pt sample there is no magnetic moment, so the suppression shown in Fig. 2(d) must originate purely from the orbital depairing effect. The Co layer in the Nb/Co/Pt sample has an IP anisotropy with an OOP saturation field of $\sim$ 120 mT [Fig. 1(a)]; the corresponding T_c plot [Fig. 2(e)] shows a rapid T_c suppression in the field range below this value, which can be partially explained by the magnetization-induced flux density being drawn OOP and adding to the applied field. A similar effect would be expected for the Nb/Pt/Co/Pt sample, albeit with a lower saturation field reflecting the OOP anisotropy [Fig. 1(b)]; in fact, the low-field suppression of T_c is lower than that for the Nb/Co/Pt sample implying that a different, partially compensating, T_c-modulating effect must be at work. This behaviour is more pronounced for Nb/Pt/Co/Pt containing a thinner 18 nm Nb [Fig. 2(f) inset]. The OOP T_c suppression is expected to be significantly larger for the following reason: in superconducting thin films, we can use Ginzburg-Landau theory to understand the magnetic field dependence of the critical temperature T_c [44]. In a perpendicular field, the upper critical $H_c(T)$ is found from

$$\frac{\mathrm{d}H_c}{\mathrm{d}T} = -\frac{\Phi_0}{2\pi T_{c0}\xi_0^2}, \tag{8}$$

where ξ_0 is the zero-temperature Ginzburg-Landau coherence length, and $\Phi_0 = h/2e$ is the flux quantum. Integrating this from zero critical field ($H_c = 0$, $T = T_{c0}$) to a finite field ($H_c = H_\perp$, $T = T_c < T_{c0}$), we find that the critical temperature reduction $\Delta T_c = T_c - T_{c0}$ due to orbital depairing follows

$$\frac{\Delta T_c}{T_{c0}} = -\frac{2\pi\xi_0^2}{\Phi_0} H_\perp. \tag{9}$$

Thus, the T_c variation with the field $H_\perp$ should depend only on the coherence length ξ_0. Fitting the observations for Nb(24)/Pt and Nb(20)/Pt, and extrapolating linearly to Nb(18)/Pt, we get an estimated $\xi_0 \approx 15.5$ nm for 18 nm Nb. We therefore expect $\Delta T_c \approx 406$ mK for Nb(18)/Pt/Co/Pt with $H_\perp = 120$ mT.

Note that the equation above ignores the additional flux injection from Co due to the magnetization rotation. To estimate a lower bound for this flux, we can rewrite Eq. (9) with the effective magnetic field $H_\perp = H_{\mathrm{ext}} + H_{\mathrm{int}}$, where H_{ext} is the external applied field, and H_{int} the internal contribution from the Co layer. Solving the resulting equation for H_{int}, we get

$$H_{\mathrm{int}} = H_{\mathrm{ext}} - \frac{\Phi_0}{2\pi\xi_0^2}\frac{\Delta T_c}{T_{c0}}. \tag{10}$$

Using the experimental ΔT_c for the Nb(24)/Co/Pt sample and $H_{\mathrm{ext}} = 120$ mT, we estimate $H_{\mathrm{int}} \approx 52$ mT, yielding a total field $H_\perp \approx 172$ mT. Applying an effective field $H_\perp = 172$ mT to Nb(18)/Pt/Co/Pt, we then estimate $\Delta T_c \approx 581$ mK, while the measured value was 380 mK. We note that the estimated value here only gives us a lower bound, since Nb(18)/Pt/Co/Pt is expected to have a larger flux injection from the Co layer than Nb/Co/Pt, due to the increased OOP anisotropy of the sample. A similar calculation for Nb(24)/Pt/Co/Pt gives an estimated $\Delta T_c \approx 420$ mK, while the measured value was 270 mK.

Taking the difference between the estimated and measured values above, we can attribute a critical temperature change of 201 mK to proximity effects in Nb(18)/Pt/Co/Pt, compared to 150 mK for Nb(24)/Pt/Co/Pt. This shows that the spin-valve effect increases significantly for thinner Nb layers.

The role of an unconventional proximity effect in the Nb/Pt/Co/Pt sample is further strengthened by the IP T_c data in Fig. 2(a–c). The data in Fig. 2(a) without a magnetic layer demonstrate small orbital depairing in the IP configuration,

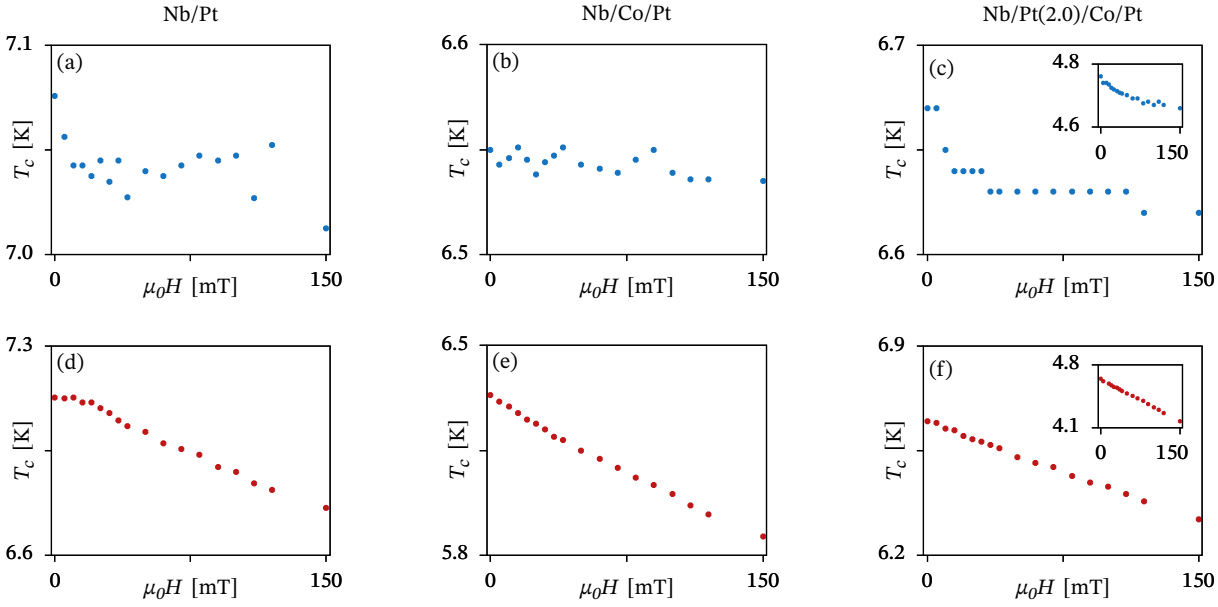

FIG. 2: Superconducting transition temperature T_c plotted against the applied field H for (a,d) Nb(24)/Pt(2), (b,e) Nb(24)/Co(1.5)/Pt(1.5), and (c,f) Nb(24)/Pt(2)/Co(1.5)/Pt(1.5). The rows correspond to IP (a-c) and OOP (d-f) applied fields. The insets in (c,f) shows the T_c vs. H plot for IP (top) and OOP (bottom) applied fields for Nb(18)/Pt(2)/Co(1.5)/Pt(1.5) having a thinner Nb layer.

resulting in $\Delta T_c < 15$ mK for $H < 120$ mT. Similar behavior is observed for the Nb/Co/Pt sample [Fig. 2(b)], for which the IP anisotropy means that an IP field does not modify the magnetic moment. In contrast, the Nb/Pt/Co/Pt sample shows a decrease in T_c of 50 mK in the same range; if this T_c modulation arose from field-induced changes to the flux injection from the Co layer, T_c should have increased since as the OOP magnetization decreased. Similar behaviour is observed for thinner Nb: T_c remains roughly constant at low IP fields for a Nb(20)/Pt(2) bilayer, but is suppressed by 90 mK for Nb(18)/Pt(2)/Co(1.5)/Pt(1.5) [Fig. 2(c) inset]. Changes arising from anisotropic interface magnetoresistance in Pt/Co/Pt structures [33, 34] can be ruled out as the resistance changes would be an order of magnitude smaller than here. To summarise: while the Nb/Pt and Nb/Co/Pt results can be qualitatively explained in terms of flux and field-induced orbital depairing, the Nb/Pt/Co/Pt behavior is distinctly different, and a rapid low-field T_c suppression is induced for IP field which tends to align the Co magnetisation parallel to the Nb plane.

The key to understanding our results is that the proximity effect in S/F systems with a single homogeneous F layer cannot be controlled by changing the magnetisation angle with respect to the film plane (after subtracting the effect of flux injection from the F layer). In S/F/F' systems, non-collinear F and F' layer moments generate LRTs, which enhance the proximity coupling between S and F and so decreases T_c. However, in our inversion asymmetric Pt/Co/Pt trilayers, we have both a magnetic field $\boldsymbol{h}$ and a Rashba coupling α in the system. As shown in Section II, this setup admits a spin-valve mechanism whereby superconductivity can be toggled on and off using the orientation of a single homogeneous magnetic layer.

IV. NUMERICS

We have modelled our results using the Usadel formalism, where we treat the Pt/Co/Pt trilayer as an effective diffusive ferromagnet with an intrinsic Rashba coupling. This approach has two advantages: firstly, scattering at Pt/Co interfaces allows us to use a diffusive model without knowing the microscopic details of the interface; secondly, the exchange splitting of the Co layer is now averaged out over a larger volume allowing us to use a quasiclassical approach. Below, we first summarize the numerical results, and then discuss the fitting procedure.

The results of the numerical simulations are shown in Fig. 3 along with a comparison with the experimental results. The difference, ΔT_c, is calculated between Nb(24)/Pt(2)/Co(1.5)/Pt(1.5) and Nb(24)/Co(1.5)/Pt(1.5) for IP and OOP fields. The figure shows the experimental and the numerically calculated ΔT_c for IP (a,b), and the corresponding plots for OOP fields (c,d). The overall numerical trend [Fig. 3(b,d)] is in excellent agreement with the experiments [Fig. 2(a,c)]. The magnitude of ΔT_c from the simulation (~ 22 mK) is 55% of that of the experimental value of 40 mK. The lower simulated values can arise due to a simplified model where we have assumed an ideal interface and a simplified magnetic model. In real systems, interdiffusion and interface roughness can affect the magnitude of ΔT_c. The shaded regions indicate the range of T_c variation in our model when the exchange field rotation range by an external field is varied. The significance of this range and the corresponding T_c variation is explained below under the discussion on magnetization modelling. But importantly, the difference ΔT_c has the right trend and order of magnitude for both IP and OOP fields. We

discuss the underlying mechanism in details in Section V. We have also compared the critical temperature difference ΔT_c between Nb/Pt/Co/Pt and Nb/Co/Pt for different Pt interlayer thicknesses which is discussed in more details in Section V.

For the numerical calculations of the critical temperature, we solved the full nonlinear diffusion equations [25],

$$iD\tilde{\nabla}(\hat{g}\tilde{\nabla}\hat{g}) = [\epsilon\hat{\tau}_z + \hat{\Delta} + \hat{h} + \hat{\kappa}\,,\, \hat{g}], \tag{11}$$

where $\hat{g}$ is the 4×4 retarded quasiclassical propagator, and $\tilde{\nabla}(\cdot) = \nabla(\cdot) - i[\hat{\boldsymbol{A}}, \cdot]$ is a gauge-covariant derivative that accounts for spin-orbit coupling. The other matrices are

$$\hat{\tau}_z = \mathrm{diag}(+1, +1, -1, -1), \tag{12}$$
$$\hat{\Delta} = \mathrm{antidiag}(+\Delta, -\Delta, +\Delta^*, -\Delta^*), \tag{13}$$
$$\hat{h} = \mathrm{diag}(\boldsymbol{h}\boldsymbol{\sigma}, \boldsymbol{h}\boldsymbol{\sigma}^*), \tag{14}$$
$$\hat{\boldsymbol{A}} = \mathrm{diag}(\boldsymbol{A}, -\boldsymbol{A}^*), \tag{15}$$
$$\hat{\kappa} = i\kappa\hat{\tau}_z\hat{g}\hat{\tau}_z. \tag{16}$$

Here, Δ is the superconducting gap, $\boldsymbol{h}$ the exchange field, $\boldsymbol{\sigma}$ the Pauli vector, $\boldsymbol{A} = \alpha(\sigma_x\boldsymbol{e}_y - \sigma_y\boldsymbol{e}_x)$ the spin-orbit field [25], and κ is a parameter that accounts for the orbital depairing [40]. To get rid of the diffusion coefficient in Eq. (11), we used that the diffusive coherence length $\xi \equiv \sqrt{D/\Delta_0} \approx 14$ nm. Using the relation $\xi \approx \sqrt{\xi_0\ell}$ for the coherence length, where $\xi_0 \approx 38$ nm is the ballistic coherence length of Nb and ℓ the mean free path of the sample, we find that this corresponds to a reasonable estimate for the mean free path $\ell \approx 5$ nm [35, 36]. The diffusion coefficient was assumed to the same in all materials.

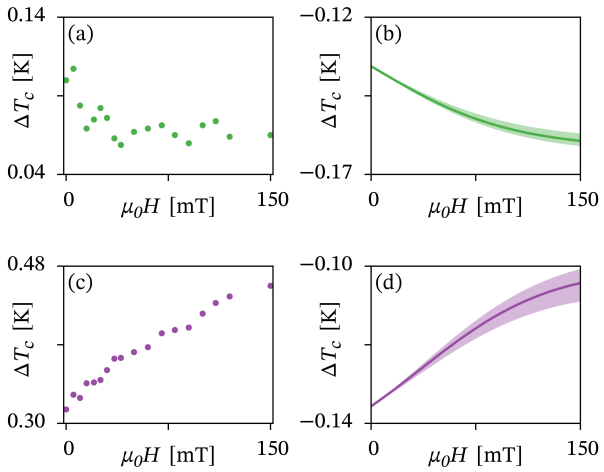

FIG. 3: Critical temperature difference ΔT_c calculated between Nb(24)/Pt(2)/Co(1.5)/Pt(1.5) and Nb(24)/Co(1.5)/Pt(1.5) as function of the applied IP and OOP fields H. The top row shows the (a) experimental and (b) simulated ΔT_c for IP fields. The corresponding OOP experimental and simulated ΔT_c is shown in (c) and (d) respectively. The solid curves (b,d) show the exchange field components for a rotation angle $\delta\theta = 30°$, while the shaded regions correspond to $\delta\theta \in [25°, 35°]$.

For the interface between the superconductor and effective ferromagnet, we used the tunneling boundary conditions [41],

$$2G_0L_{\mathrm{L}}\hat{g}_{\mathrm{L}}\partial_z\hat{g}_{\mathrm{L}} = 2G_0L_{\mathrm{R}}\hat{g}_{\mathrm{R}}\partial_z\hat{g}_{\mathrm{R}} = G_T[\hat{g}_{\mathrm{L}}\,,\,\hat{g}_{\mathrm{R}}], \tag{17}$$

where G_0 is the normal-state conductance of each material, G_T is the tunneling conductance of the interface, $\hat{g}_{\mathrm{L,R}}$ are the propagators on the left and right side of the interface, respectively, and $L_{\mathrm{L,R}}$ are the corresponding material lengths. The tunnel conductance between the superconductor and effective ferromagnets was determined by calculating the critical temperature T_c/T_{cs} in the absence of an external field, and selecting the best possible values for the conductance ratio G_T/G_0. We simultaneously tried to make sure that the ratio between T_c for Nb/Co/Pt and Nb/Pt/Co/Pt was as close to the experimental values as possible. Unfortunately, we were unable to get a perfect quantitative fit using reasonable parameters here; but using $G_T/G_0 = 0.65$ for Nb/Co/Pt and $G_T/G_0 = 0.85$ for Nb/Pt/Co/Pt did provide a qualitative match. Note that we assume the normal-state conductance G_0 to be the same in Nb and the [Pt]/Co/Pt heterostructure. In reality, these two are different, and estimating an effective G_0 for the heterostructure from known parameters is not straight-forward. However, a difference in the normal-state conductances of the materials simply decreases the proximity-effect [2], and the same happens if the tunneling conductance is decreased. Thus, we may compensate for a conductance asymmetry by adjusting G_T accordingly—and since the tunneling conductance is already treated as a fitting parameter, this happens automatically.

In order to self-consistently determine the superconducting properties of a hybrid structure, we not only require equations for the propagator $\hat{g}$, but also an accompanying equation for the superconducting gap Δ. This equation can be written [25]

$$\Delta = \frac{1}{\log(2\omega_c/\Delta_0)}\int_0^{\omega_c} \mathrm{d}\epsilon\ \mathrm{Re}[f_s]\tanh\left(\frac{\pi}{2e^\gamma}\frac{\epsilon/\Delta_0}{T/T_{cs}}\right), \tag{18}$$

where ω_c is the Debye cutoff energy, Δ_0 the zero-temperature gap of a bulk superconductor, T_{cs} the critical temperature of a bulk superconductor, and γ the Euler–Mascheroni constant. We used $\omega_c = 30\Delta_0$ in our simulations, and for Nb the relevant material constants are $\Delta_0 \approx 1.4$ meV and $T_{cs} \approx 9.2$ K. In the numerical implementation, we use a Riccati-parametrization for the propagator $\hat{g}$, and employ a kind of binary search algorithm for the calculation of the critical temperature T_c. For more details about this numerical procedure, see Ref. 42.

The magnetization was modelled as follows. The measured magnetization was found to roughly follow the profile

$$M = M_0 + \delta M\tanh(H/H_0), \tag{19}$$

where M is the magnetization component along the applied field H. This suggests that we model the exchange field as

$$h_x/h_0 = \cos(\theta_0) + [\cos(\theta_0 - \delta\theta) - \cos(\theta_0)]\tanh(H/H_0) \tag{20}$$

in the case of an IP applied field H, and

$$h_z/h_0 = \sin(\theta_0) + [\sin(\theta_0 + \delta\theta) - \sin(\theta_0)]\tanh(H/H_0) \tag{21}$$

for an OOP applied field H. In both cases, we have assumed that the exchange field remains in the xz-plane, so that the relation $h_x^2+h_z^2 = h_0^2$ can be used to find the other component. Here, θ_0 is interpreted as the angle that the exchange field direction makes with the thin-film plane in the absence of external fields, while $\delta\theta$ parametrizes the maximum exchange field rotation that can be achieved using an external field. Based on the experimental measurements, we found the saturation parameter $H_0 \approx 100$ mT to fit the data very well, but estimating θ_0 and $\delta\theta$ turned out to be difficult. We therefore fixed the first parameter to $\theta_0 = 45°$, and varied $\delta\theta \in [25°, 35°]$ to see how the results change, since the critical temperature T_c is more sensitive to variations in $\delta\theta$ than θ_0. Finally, assumed an average exchange field $h_0 = 100\Delta_0 \approx 140$ meV for the Pt/Co/Pt heterostructure, based on previously reported values of 300 meV for Co [37]. Using the model above, we have plotted the resulting exchange field $\boldsymbol{h}$ as a function of the applied field H in Fig. 4.

Next, we discuss the orbital depairing effect. For thin-film systems, the depairing effect usually causes the critical temperature to decrease linearly with the applied field when the external field is applied OOP, and quadratically when the external field is applied IP [43]. These two cases correspond to the depairing parameters $\kappa = \Delta_0(H/H_c)$ and $\kappa = \Delta_0(H/H_c)^2$, respectively, where H_c is a critical field for which $T_c \to 0$ in the absence of proximity effects. From the experimental results, we see that for an OOP case we do get a linear decrease in T_c as expected. By fitting the critical temperature decay $T_c(H = 120\text{ mT})/T_c(H = 0)$ that we get from the numerical simulations to that in the Nb/Co/Pt experiment, we get an estimate $H_c \approx 1.8$ T for the critical field. For the Nb/Pt/Co/Pt structure, we simply assumed that the orbital depairing effect was the same as for Nb/Co/Pt. For the case of an IP applied field, however, we see from the experiment that the orbital depairing is negligible for $H < 150$ mT, and was therefore excluded from the IP models (i.e. $H_c = \infty$).

Finally, we estimated the Rashba coupling $\alpha \approx 12$ by fitting the ratio $T_c(H = 120\text{ mT})/T_c(H = 0)$ for the Nb/Pt/Co/Pt structures, and selecting the value of α that produces the best possible fits for both the IP and OOP case. This is in the unit $\hbar^2/m\xi$, where m is the electron mass and $\hbar$ is Planck's reduced constant; restoring the units we get $\alpha \approx 6.5 \times 10^{-11}$ eV·m, which is very close to previous experimental estimates. This value is close to $\sim 5 \times 10^{-12}$ eVm for asymmetric Pt/Co/Pt structures estimated from Ref. 38. The higher values in our system could arise due to different Pt and Co thicknesses and interfaces, which strongly influence the Rashba coupling [29].

V. DISCUSSION

In the previous section, a comparison of the experimental results with the numerical calculation shows that the T_c suppression for OOP fields for Nb(24)/Co(1.5)/Pt(1.5) is purely due to orbital effects. The Pt layer at the Nb/Co interface in Nb/Pt/Co/Pt therefore plays an important role. This is most strikingly evident in the ΔT_c between Nb/Co/Pt and Nb/Pt Fig. 5. The IP ΔT_c (Fig. 5a) remains constant ($\sim$ 10 mK fluctuation) whereas the OOP ΔT_c (Fig. 5b) decreases with

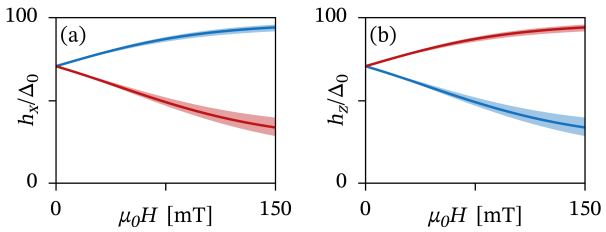

FIG. 4: Plot of the (a) IP and (b) OOP exchange field in our numerical model as functions of the applied field H. The blue curves correspond to an IP applied field, and the red curves an OOP applied field. The solid curves show the exchange field components for a rotation angle $\delta\theta = 30°$, while the shaded regions correspond to $\delta\theta \in [25°, 35°]$.

increasing applied field, in sharp contrast with Nb/Pt/Co/Pt structures. This can easily be explained by equal negligible orbital depairing for IP fields in both structures and increased flux injection in Nb/Co/Pt for OOP fields which suppresses the T_c more rapidly for Nb/Co/Pt.

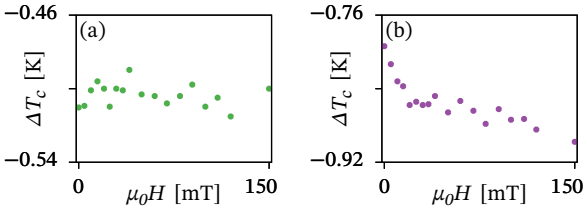

FIG. 5: Critical temperature difference ΔT_c calculated between Nb(24)/Co(1.5)/Pt(1.5) and Nb(24)/Pt(1.5) as function of the applied (a) IP and (b) OOP fields H.

However, in Nb(24)/Pt(2)/Co(1.5)/Pt(1.5) there is a compensating effect due to suppression of the spin-zero triplet (short-ranged triplets, SRT) generation resulting in an increasing ΔT_c with the applied field. For IP fields with negligible orbital depairing, ΔT_c decreases due to an enhancement of the proximity effect in Nb(24)/Pt(2)/Co(1.5)/Pt(1.5) arising from an increased SRT generation. To better understand the role of the Pt layer at the Nb/Co interface, we have examined T_c variation with the thickness of this layer. In Figure 6, we plot the ΔT_c between Nb(24)/Pt(x)/Co(1.5)/Pt(1.5) and Nb(24)/Co(1.5)/Pt(1.5) for $x = 0.3$ and $x = 1$ and the results of the numerical simulation for these structures. While for IP fields ΔT_c is $\sim$ 15 mK for 0.3 nm [Fig. 6(a)], the 1 nm structure shows $\sim$ 25 mK drop superimposed on the noise [Fig. 6(b)]. The fitting process described in Section IV has been repeated for Pt interlayers of thickness 0.3 nm and 1.0 nm, in place of the 2.0 nm interlayer discussed above. The simulated ΔT_c values [Fig. 6 e,f] are in reasonable agreement with the experimental data. For the 0.3 nm case, we found a reduced Rashba coupling $\alpha \approx 9$, and the same tunneling conductance as for Nb/Co/Pt. For the 1.0 nm case, however, both these parameters were the same as for the 2.0 nm case.

The ΔT_c trend with Pt thickness becomes clear when they

are compared with the $M(H)$ loops [Fig. 7] for these samples. With increasing Pt layer thickness from 0.3 nm to 1 nm, the magnetisation gradually changes fully IP [Fig. 7(a)] with OOP hard axis [Fig. 7(c)] to a clear hysteretic switching for both IP and OOP [Fig. 7(b,d)]. This develops further when the bottom Pt thickness is increased to 2 nm as seen from Fig. 1. The corresponding IP field-dependent T_c for 2 nm Pt shows a large change $\sim$50 mK at low fields [Fig. 2(c)].

The large change in low-field T_c appears only in the region where the IP magnetization approaches saturation, beyond which the T_c suppression is comparable for all the structures. This indicates the active role played by the magnetization angle in modulating T_c for structures showing a comparable IP and OOP anisotropy in addition to the presence of a Pt layer at the Nb/Co interface. ΔT_c for the OOP field [Fig. 6(c,d)] increases with applied field and similar to the IP ΔT_c [Fig. 6(a,b)], the magnitude of this change increases with thicker Pt layer at the Nb/Co interface. Our measurements possibly underestimate the magnitude of the SOC-induced change. This is because the increased OOP magnetisation with increasing x in Nb/Pt(x)/Co/Pt results in more Co flux being directed into Nb. This reduces T_c as x is increased, which can counteract some of the T_c increase caused by the stronger SOC associated with increasing x. This implies that even though we see a finite non-zero T_c for OOP fields for $x = 0.3$ and $x = 1.0$, the actual SOC-induced changes get progressively higher with increasing

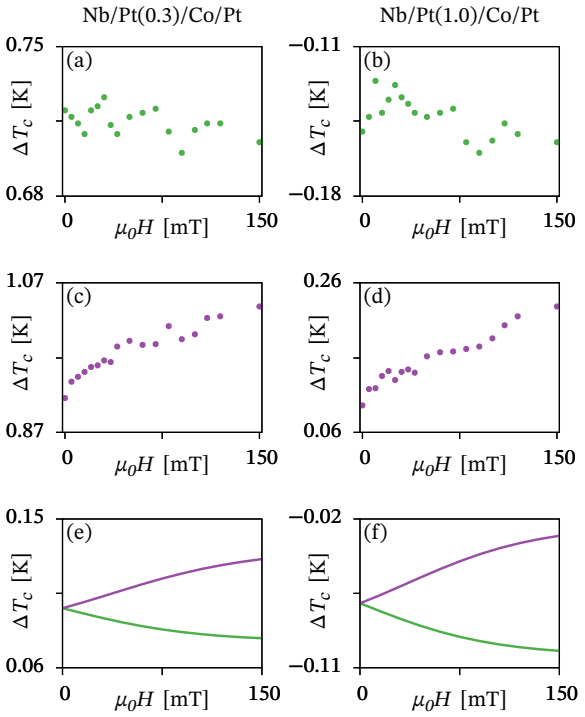

FIG. 6: Critical temperature difference ΔT_c between Nb(24)/Pt(x)/Co(1.5)/Pt(1.5) and Nb(24)/Co(1.5)/Pt(1.5) as function of the applied field H. The columns correspond to $x = 0.3$ and $x = 1.0$. The rows correspond to IP fields, OOP fields, and numerical simulations.

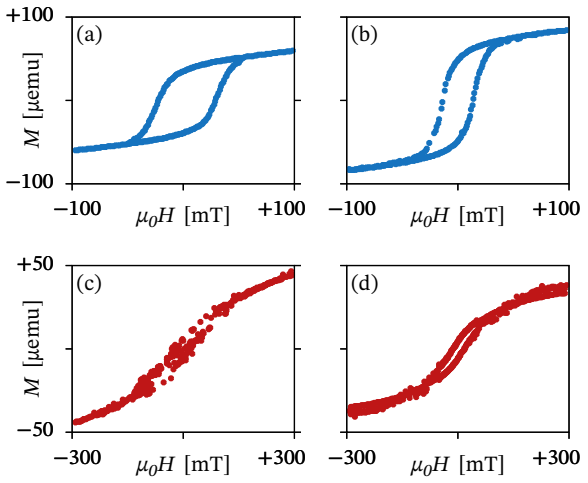

FIG. 7: Magnetization M as function of the applied field H. The left column shows results for Nb/Pt(0.3)/Co/Pt, and the right column results for Nb/Pt(1.0)/Co/Pt. The top row corresponds to IP applied fields, while the bottom row corresponds to OOP applied fields.

Pt thickness to compensate for the increasing flux injection from OOP magnetisation. SOC introduces two competing effects: triplet depairing due to imaginary terms in the effective energy, and LRT generation due to triplet mixing terms [25]. Numerically we found the energy-penalty of the SRT is more important than the LRT generation for the T_c modulation. We reiterate an important point: SOC couples the magnetization with the SRT energy, which is different to spin-relaxation effects induced by SOC on superconductivity [35].

In S/F structures without SOC, the SRT energy is independent of the magnetization state, and T_c is independent of the magnetization angle θ. However, in presence of SOC the SRT energy depends on T_c; with an increasing OOP field, the "leakage" of the Cooper pairs through the triplet channel is reduced, thereby increasing the T_c (since the superconducting gap directly depends on the singlet pair amplitude). As the magnetization is made IP, the SRT generation is energetically more favourable, thereby "draining" the superconductor of Cooper pairs and reducing T_c. The triplet Cooper pairs are not confined to the ferromagnetic region, but are also expected to exist in the Nb region near the interface. However, an explicit demonstration of this would require e.g. local STM-measurements which is outside of the scope of the present work. There is thus a qualitative difference between the samples for which SOC is expected to be relevant and those which simply have a magnetic layer whose magnetic orientation controls the injected flux.

VI. CONCLUSION

The results reported here cannot be explained by conventional S/F proximity theory without considering SOC. While the superconducting spin-valve with a single homogeneous ferro-

magnet demonstrated here drastically simplifies the control of superconductivity, a natural progression involves structures with combined Rashba and Dresselhaus coupling predicted to control LRT [25]. Incorporating such structures in Josephson junctions would allow the design of devices currently under intense focus in superspintronics.

[1] A.I. Buzdin. *Rev. Mod. Phys.* **77**, 935 (2005).
[2] F.S. Bergeret, A.F. Volkov, K.B. Efetov. *Reviews of Modern Physics* **77**, 1321 (2005).
[3] L. Lazar, K. Westerholt, H. Zabel. *Phys. Rev. B* **61**, 3711 (2000).
[4] J.S. Jiang, D. Davidović, D.H. Reich, C.L. Chien. *Phys. Rev. Lett.* **74**, 314 (1995).
[5] L.R. Tagirov. *Phys. Rev. Lett.* **83**, 2058 (1999).
[6] I. Baladié, A. Buzdin, N. Ryzhanova, A. Vedyayev. *Phys. Rev. B* **63**, 054518 (2001).
[7] A.I. Buzdin, A. Vedyayev, N.V. Ryzhanova. *Europhys. Lett.* **686**, 6 (1999).
[8] P.V. Leksin, N.N. Garif'yanov, I.A. Garifullin, Y.V. Fominov, J. Schumann, Y. Krupskaya, V. Kataev, O.G. Schmidt, B. Büchner. *Phys. Rev. Lett.* **109**, 057005 (2012).
[9] V.I. Zdravkov, J. Kehrle, G. Obermeier, D. Lenk, H.A. Krug von Nidda, C. Müller, M.Y. Kupriyanov, A.S. Sidorenko, S. Horn, R. Tidecks, L.R. Tagirov. *Phys. Rev. B* **87**, 144507 (2013).
[10] X.L. Wang, A. Di Bernardo, N. Banerjee, A. Wells, F.S. Bergeret, M.G. Blamire, J.W.A. Robinson. *Phys. Rev. B* **89**, 140508(R) (2014).
[11] A. Singh, S. Voltan, K. Lahabi, J. Aarts. *Phys. Rev. X* **5**, 021019 (2015).
[12] M. Houzet, A.I. Buzdin. *Phys. Rev. B* **76**, 060504(R) (2007).
[13] J. Linder, J.W.A. Robinson. *Nat. Phys.* **11**, 307 (2015).
[14] M. Eschrig. *Phys. Today* **64**, 43 (2011).
[15] J.W.A. Robinson, J.D.S. Witt, M.G. Blamire. *Science* **329**, 59 (2010).
[16] T.S. Khaire, M.A. Khasawneh, W.P. Pratt, N.O. Birge. *Phys. Rev. Lett.* **104**, 137002 (2010).
[17] N. Banerjee, C.B. Smiet, R.G.J. Smits, A. Ozaeta, F.S. Bergeret, M.G. Blamire, J.W.A. Robinson. *Nat. Commun.* **5**, 3048 (2014).
[18] N. Banerjee, J.W.A. Robinson, M.G. Blamire. *Nat. Commun.* **5**, 4771 (2014).
[19] M.G. Blamire, C.B. Smiet, N. Banerjee, J.W.A. Robinson. *Supercond. Sci. Technol.* **26**, 55017 (2013).
[20] L.P. Gor'kov, E.I. Rashba. *Phys. Rev. Lett.* **87**, 37004 (2001).
[21] G. Annunziata, D. Manske, J. Linder. *Phys. Rev. B.* **86**, 174514 (2012).
[22] F.S. Bergeret, I.V. Tokatly. *Phys. Rev. Lett.* **110**, 117003 (2013).
[23] A.P. MacKenzie, Y. Maeno. *Rev. Mod. Phys.* **75** 657 (2003).
[24] F.S. Bergeret, I.V. Tokatly. *Phys. Rev. B.* **89**, 134517 (2014).
[25] S.H. Jacobsen, J.A. Ouassou, J. Linder. *Phys. Rev. B. Phys.* **92**, 024510 (2015).
[26] V.M. Edelstein. *Phys. Rev. B* **67**, 020505 (2003).
[27] V.M. Edelstein. *Pis'ma v ZhETF* **77**, 212 (2003).
[28] P.P.J. Haazen, E. Murè, J.H. Franken, R. Lavrijsen, H.J.M. Swagten, B. Koopmans. *Nat. Mater.* **12**, 299 (2013).
[29] R. Lavrijsen, D.M.F. Hartmann, A. van den Brink, Y. Yin, B. Barcones, R.A. Duine, M.A. Verheijen, H.J.M. Swagten, B. Koopmans. *Phys. Rev.* **B 91**, 104414 (2015).
[30] N. Nakajima, T. Koide, T. Shidara, H. Miyauchi, H. Fukutani, A. Fujimori, K. Iio, T. Katayama, M. Nývlt, Y. Suzuki. *Phys. Rev. Lett.* **81**, 5229 (1998).
[31] S. Bandiera, R.C. Sousa, B. Rodmacq, B. Dieny. *IEEE Magn. Lett.* **2**, 3000504 (2011).
[32] T. Ueno, J. Sinha, N. Inami, Y. Takeichi, S. Mitani, K. Ono, M. Hayashi. *Sci. Rep.* **5**, 14858 (2015).
[33] A. Kobs, S. Heße, W. Kreuzpaintner, G. Winkler, D. Lott, P. Weinberger, A. Schreyer, H.P. Oepen. *Phys. Rev. Lett.* **106**, 217207 (2011).
[34] Y.M. Lu, J.W. Cai, S.Y. Huang, D. Qu, B.F. Miao, C.L. Chien. *Phys. Rev. B.* **87**, 220409(R) (2013).
[35] J. Draskovic, T.R. Lemberger, B. Peters, F. Yang, J. Ku, A. Bezryadin, S. Wang. *Phys. Rev. B.* **88**, 134516 (2013).
[36] C. Delacour, L. Ortega, M. Faucher, T. Crozes, T. Fournier, B. Pannetier, V. Bouchiat. *Phys. Rev. B.* **83**, 144504 (2011).
[37] J.W.A. Robinson, S. Piano, G. Burnell, C. Bell, M.G. Blamire. *Phys. Rev. Lett.* **97**, 177003 (2006).
[38] S.T. Lo, S.W. Lin, Y.T. Wang, S.D. Lin, C.T. Liang. *Sci. Rep.* **4**, 5438 (2014).
[39] K.D. Usadel. *Physical Review Letters* **25** 507 (1970).
[40] M. Silaev, P. Virtanen, F.S. Bergeret, T.T. Heikkilä. *Physical Review Letters* **114** 167002 (2015).
[41] M.Y. Kuprianov, V.F. Lukichev. *Soviet Physics JETP* **67** 1163 (1988).
[42] J.A. Ouassou, A. Di Bernardo, J.W.A. Robinson, J. Linder. *Nature Scientific Reports* **6** 29312 (2016).
[43] R. Meservey, P.M. Tedrow. *Physics Reports* **238** 173 (1994).
[44] S.I. Krasnosvobodtsev, N.P. Shabanova, E.V. Ekimov, V.S. Nozdrin, E.V. Pechen. *Sov. Phys. JETP* **81**, 534 (1995).